Supplemental Materials
for
Heterochronic shifts and conserved embryonic shape underlie crocodylian craniofacial disparity and convergence

Supplementary Methods

Description of Landmarks

Landmarks were chosen to maximize both the amount of shape captured and the number of embryos to be included in the analysis. We restricted our landmarks to only type I or II (*sensu* Bookstein, 1991) as described in the list below. However, the inclusion of the poorly ossified skulls of embryos required that some points be placed with slightly modified criteria. Specifically, landmarks positioned on sutures (landmarks 8-10, 13, & 14) were placed principally on the bolded element when sutural contact was weak. Additionally landmark 4 was placed along the midline at the position of the most posterior point of the skull roof, even if that point was not on the midline anatomically. Positions of discrete landmarks are shown in electronic supplementary figure S1. Landmarking was conducted using the TPS suite of programs.

Landmarks

1. Anterior extent of premaxilla along the midline
2. Anterior extent of nasal along the midline
3. Anterior extent of frontal along the midline
4. Posterior extent of supraoccipital along the midline
5. Posteromedial most extent of the supratemporal fenestra and fossa
6. Anterolateral most extent of the supratemporal fenestra and fossa
7. Posterolateral most extent of the skull roof portion of the squamosal
8. Posterior extent of the suture between **quadrate** and quadratojugal
9. Posterior extent of the suture between **quadratojugal** and jugal
10. Posterolateral extent of the suture between the **jugal** and maxilla
11. Posterior most extent of the bony orbit
12. Anterior most extent of the bony orbit
13. Anteriormedial most extent of the suture between the **maxilla** and nasal (often the tripartite contact with the premaxilla)
14. Lateral extent of the suture between the **premaxilla** and maxilla (or posterolateral extent of premaxilla)

Citations:

Bookstein, F. L. (1991). Morphometric Tools for Landmark Data: Geometry and Biology. Cambridge: Cambridge University Press.

Landmarking Methods

To ensure accuracy and reproducibility of landmark placement, a subset of specimens were landmarked multiple times by one individual (ZSM). This landmark dataset was imported into R using *geomorph* functions and overlap of raw coordinates for each species were assessed to determine accuracy and reproducibility.

R code

The code used in this analysis, along with the TPS and CSV files containing landmark and covariate data, can be found in the R package supplementary file hosted on Dryad (Data available from the Dryad Digital Repository: https://doi.org/10.5061/dryad.6cv82g1). The major functions used in this analysis were:

- *gpagen* - performs a general Procrustes alignment of raw coordinates
- *plotTangentSpace* & *prcomp* - takes Procrustes aligned coordinates and performs principle components analysis (PCA); plotTangentSpace also creates a PCA plot
- *advanced.procD.lm* - compares two models of factors which may explain variation in Procrustes coordinates. This was used to compare how skull shape varies with ontogenetic period and ecomorph classification and perform pairwise comparisons among ontogenetic periods and ecomorphs.
- *morph.disparity* - estimates morphological disparity by calculating Procrustes variance around the mean shape of each group and performs pairwise comparisons using resampling to assess significance. We used this to compare disparity among ecomorphs and ontogenetic periods.
- *procD.allometry* - calculates allometric regression of Procrustes aligned coordinates on a continuous measure of size (i.e., log(centroid size)) and uses resampling to test whether allometric trajectories differ among groups (a covariate). We used this analysis to compare trajectories across all species and also in pairwise comparisons.
- *p.adjust* - a function which can take a significance level and a number of comparisons to calculate an adjusted p-value given the repeated testing. We use this to properly adjust our pairwise procD.allometry analyses.
- *lm* - a general linear model function which was used to perform linear regression of PC scores (all PCs) against log(centroid size). This was used to extract slope and intercept coefficients for the ontogenetic trajectory projected along each PC for ancestral state reconstruction.
- *contMap* - uses a maximum likelihood algorithm for ancestral state reconstruction of continuous traits at all nodes in a phylogeny and maps changes along branches in the phylogeny. We used this to calculate and map the changes in slope and intercept coefficients along PCs.
- *anc.ML* - a maximum likelihood function which estimates the evolutionary parameters and ancestral states for Brownian evolution. This method was employed within *contMap* for our analyses.

CT scanning and processing methods

CT scans were generated using the Harvard CNS or Natural History Museum, London micro-CT systems (both X-Tek HMX ST 225) with a Molybdenum target. Scan parameters were set to maximize useful contrast individually for each scan (Data available from the Dryad Digital Repository: https://doi.org/10.5061/dryad.6cv82g1). CT scan reconstruction was conducted using CT 3D pro (X-Tek), verifying appropriate reconstruction of center of rotation and cropping projection images. CT scans were imported into VGStudio Max 2.3 (Volume Graphics GmbH, Heidelberg,

Germany) for further processing. Using the specific histogram of gray values for each specimen, the opacity of gray values was modulated in order to minimize non-skeletal materials (air, ethanol filled soft-tissue) and noise. Segmenting of bony elements, and identification of the position and edges of developing bone, was done using a combination of gray scale values and visual assessment of texture after thresholding to remove non-skeletal materials. The segmented skulls were then extracted and positioned for imaging in dorsal view.

Supplementary Analyses

Landmark Assessment

The inclusion of embryonic (non-skeletally mature) specimens in our analysis necessitated reducing the number of landmarks as compared to prior studies based on post-hatching specimen (e.g. Pierce et al. 2008; Sadlier 2009; Piras et al. 2010; Watanabe and Slice 2014). To ensure that reducing the number of landmarks did not dramatically affect the distribution of species and/or ecomorphs in morphospace, we ran a validation test using the dataset from Pierce et al. (2008). We generated two morphospaces: one with the full complement of landmarks from the original analysis, and one in which landmarks were removed to match the 14 landmarks used in our analysis (electronic supplementary figure S2). Our validation test demonstrated that reducing the number of landmarks resulted in a similar distribution of species/ecomorphs in morphospace, as well as similar axes of shape variation. This result indicates that our landmarking scheme accurately captures variation in skull shape and provides confidence for including embryonic material in our analysis of crocodylian craniofacial ontogenetic evolution.

Adult & Subadult Morphospace & Ecomorphotype Categorization

Previous studies have divided extant crocodylians into surprisingly different ecomorphotypes, even while providing similar descriptions of these categories (e.g., Brochu, 2001; McHenry et al., 2006). To understand adult skull shape and ecomorphotype, we subsampled our total ontogeny dataset and performed PCA on only the adult and subadult specimens for all 23 species of crocodylians (n = 155; electronic supplementary table S1). We then assessed the ecomorph categorizations of previous studies (McHenry et al., 2006; Pierce et al., 2008).

Although there are overlapping edges, distinct clusters are apparent in the smear of non-gavialoid crocodylians in the adult/subadult morphospace. A “moderate” ecomorph is centered just to the upper left of the origin, a “blunt” ecomorph falls to the more negative values, and “slender” forms have the most positive PC values. Electronic supplementary table S2 shows the various ecomorph classifications for all species in previous analyses and the classifications assigned in this study. We started from the classification of McHenry and colleagues (2006), but based on position in our adult/subadult morphospace we assigned classifications and reclassified several species.

Tomistoma and *Gavialis* fall to the PC1 positive extreme. However, given the classical inclusion of both species as “longirostrine”, we maintained them in the “slender” ecomorph alongside *Mecistops* and *Crocodylus johnstoni. Crocodylus acutus*, *C. intermedius*, and C*. novaguineae* were all categorized as “mesorostrine” by McHenry and colleagues, but similar to the results of Pierce and colleagues (2008) we recognized all three as “slender”.

Although *Caiman latirostris* has been classified as “brevirostrine” previously, both *Caiman crocodilus* and *Caiman yacare* were not explicitly classified by McHenry and colleagues (2006). Previous GMM analysis recognized all three of these species as occupying the “Short & Broad” quadrant of morphospace (Pierce et al., 2008). *Caiman crocodilus* and *Caiman yacare* have less broad faces compared to *Caiman latirostris* and occupy a position in between the rest of either the “moderate” or “blunt” species in the adult/subadult morphospace (electronic supplementary figure S3). Given this similarity, we placed all three species of *Caiman* in the “blunt” ecomorph.

Additionally, *Melanosuchus* clearly overlaps with *Caiman latirostris* and *Osteolaemus* and belongs in the "blunt" ecomorph despite previously being considered "mesorostrine".

Alligator sinensis, *Paleosuchus trigonatus*, and *P. palpebrosus* were all classified as "brevirostrine", but our data suggest that they actually have skulls more similar to "moderate" forms than previously recognized. *Alligator sinensis* overlaps with *A. mississippiensis* and *P. Trigonatus* is actually closer to the center of the moderate ecomorph cluster than either species of *Alligator*. *Paleosuchus palpebrosus* is actually the closets to the blunt ecomorph.

ANOVA revealed that these groups all are significantly different in their morphospace occupation, across all classification schemes (p-values < 0.01). Our classification scheme is used primarily for ease of comparing relatively similar adult cranial shapes, but did not limit downstream analysis as all comparisons of ontogenetic trajectories were made across all species.

Evolutionary trends of cranial ontogeny in subclades

From the ancestral crocodylian the two major subclades in the molecular preferred topology, Alligatoridae and Crocodylidae+Gavalidae, show opposite changes in PC1 trajectory elevation (Figure 4). The ancestral alligatorid (node 2g; electronic supplementary figures S4, 10-12) has a decreased PC1 elevation (post-displacement) and slightly increased PC2 slope (acceleration), whereas the ancestor of crocodylids and gavalids (node 8g) shows the opposite elevation shift relative to the ancestral crocodylian (node 1g). Whereas the Caimaninae lineage underwent changes in ontogeny to achieve blunt skull shapes (see main text), the genus *Alligator* maintains the moderate ecomorph. Prior to the split within *Alligator* (node 3g), no change was recovered to PC1 or PC2 ontogeny. Subsequently, *A. sinensis* underwent a combination of PC1 slope increase (acceleration) and PC2 elevation shift (pre-displacement) which resulted in shorter and wider embryonic skull shapes but similar adult skull shape. In contrast, *A. mississippiensis* only shows a decreased PC1 slope (deceleration) to give its slightly less triangular face as adults.

After the divergence of the gavialids, the lineage leading to *Crocodylus* (between nodes 8g & 10g) sees a minor decrease in PC1 elevation (post-displacement) and a moderate increase in PC2 slope (acceleration). This branch leads to a node which is partially equivalent to both the crocodylidae and crocodylinae nodes, as it is both the most inclusive clade which contains *Crocodylus* but not *Gavialis* (i.e., crocodylidae) and the most inclusive clade which contains *Crocodylus* but not *Tomistoma* (i.e, crocodylinae). Interestingly, the two shifts in PC1 elevation from the ancestral crocodylian (node 1g) to this ancestral crocodylid (node 10g) are of equal magnitude but opposite direction such that their ontogenetic trajectories are virtually identical. From this node, no change in trajectory is recovered in the lineage leading to the ancestor of *Mecistops* and *Osteolaemus* (node 11g). The sister lineage is the genus *Crocodylus* (node 12g), which underwent a slight decrease in PC1 slope (deceleration) and an very slight decrease in PC2 elevation (post-displacement). Within *Crocodylus*, our analysis did not recover any shifts in ontogeny between nodes 12g, 13g, and 16g, while only a minor PC2 slope decrease (deceleration) occurred between 13g and 14g. The internal branches between 14g & 15g and 16g & 17g showed additional minor PC1 accelerations. Along the terminal branches several significant shifts were recovered which did not change out of the moderate ecomorph (figure 4; electronic supplementary figure S12).

Evolutionary trends of cranial ontogeny in the morphological topology

In the morphological topology (electronic supplementary figures S4, 10-11), alligatorids and crocodylids form the clade Brevirostres which breaks up some of the early heterochronic shifts observed in the reconstruction based on the molecular topology. The PC1 post-displacement and PC2 acceleration events leading to the alligatorid ancestor are spread across two different branches, with the first one leading to Brevirostres (node 2m). While the second shifts result in the same ancestral ontogenetic trajectory reconstruction for Alligatoridae (node 3m), no shifts are recovered leading to the Crocodylidae (node 9m). The branch leading to *Alligator* (node 4m) shows minor PC1 slope decrease (deceleration) instead of on the *A. mississippiensis* terminal branch. Otherwise, trends are the same as the reconstruction based on the molecular phylogeny.

Within Crocodylidae, there are several more internal nodes leading up to the genus *Crocodylus* (node 12m) than in the molecular topology because *Tomistoma*, *Osteolaemus*, and *Mecistops* all fall as progressive outgroups. This complicates comparison of nodes between topologies. However, nodes 10g and 10m (i.e., Crocodylinae) have virtually identical ontogenetic trajectories. The terminal branch leading to *Osteolaemus* shows the same shifts as in the molecular tree, but the *Mecistops* terminal branch finds support for PC2 elevation decrease (post-displacment) instead of slope decrease (figure 4). The *Tomistoma* terminal branch underwent PC1 intercept increase (pre-displacement) and PC2 intercept decrease (post-displacement) not seen in the molecular tree. Clearly, the sister taxon relationship of *Gavialis* and *Tomistoma* pushes PC1 pre-displacement and PC2 deceleration to their common ancestor in the molecular reconstruction which is divided in the morphological reconstruction. Although significant differences between tip species and the backbone nodes between Crocodylidae and *Crocodylus* (nodes 9m, 10m, 11m, and 12m) are recovered, it is ambiguous how these shifts are optimized on the tree (electronic supplementary table S14). However, overall a slightly decreased elevation for PC1 and increased elevation for PC2 ontogenies occur across this series of nodes.

Within *Crocodylus*, species fall into two diverging lineages (*C. palustris*, *C. siamensis*, *C. porosus*, and *C. novaeguineae* sharing node 13m and *C. moreletii*, *C. rhombifer*, and *C. niloticus* sharing node 16m). Overall, changes to ontogeny are minor within the genus and those that occur primarily modify embryonic skull shape, not adult skull shape. *Crocodylus niloticus* & ancestral node 16m are indistinguishable from the *Crocodylus* ancestor (node 12m). However, PC1 & 2 acceleration occurs from 16m to 17m. Subsequently *C. rhombifer* and *C. moreletii* diverge in embryonic shape (PC1 pre-displacement vs. post-displacement and PC2 pre-displacement vs. acceleration, respectively). All significant shifts within the 13m clade appear to be optimized on terminal branches, with the exception of one potential deceleration event prior to the splitting of *C. novaguineae* and *C. porosus* (node 14m to 15m). Beyond this there is support for PC1 post-displacement leading to *C. palustris* and PC1 and PC2 acceleration leading to *C. siamensis*. Surprisingly, *C. novaguineae* has a significantly steeper PC1 slope than it's nearest ancestral node (15m), finding support for acceleration not recovered with the molecular topology (figure 4; electronic supplementary table 14).

Supplementary Tables

All tables are included as separate pages within the "Morris_CrocodylianHeterochrony_SI_Tables" pdf files. Table Captions are provided below.

Table S1. Sampling of species and ontogenetic stages

List of the species included in the total ontogeny PCA and the number of specimens sampled per developmental period for each species. Asterisks represent species for which at least one embryo was sampled, while crosses represent species for which at least one hatchling was sampled. "Embryonic" includes mid-stage embryos and late-stage embryos, while "post hatching" includes and hatchlings, juveniles, subadults, and adults.

Table S2. Ecomorphotype classifications

Comparisons of the crocodylian ecomorphotype classifications schemes of McHenry and colleagues (2006), and Pierce and colleagues (2008), and this study. Bolded species were reclassified based on our PCA of adults and subadults and underlined taxa are those not previously assigned by McHenry and colleagues (2006).

Table S3. Principal component loadings and correlations with CAC

The list of principal components resulting from the total ontogeny PCA, the proportion of variance explained by each PC, the cumulative proportion of shape variance and the standard deviation. The last two columns give the results of the test of the correlation between PCs and common allometric component (CAC) scores generated from *procD.allometry* (Cor and p-value).

Table S4. Comparison of skull shape among ecomorphs

Results of the Procrustes ANOVA comparisons of skull shape among ecomorph groups, within different ontogenetic periods (adults/subadults, juveniles, hatchlings, late-skeletal and mid-skeletal period embryos) and the total dataset. The least squares distance between the mean shape of stages are given on the bottom triangle and the p-value given above. Results reveal that ecomorphs differ significantly among the adults/subadults and total dataset comparisons, but mid-skeletal period ecomorphs are not significantly different.

Table S5. Comparison of skull shape disparity across ontogeny

Results of pairwise comparison of shape disparity among different ontogenetic periods, excluding *Gavialis*. Procrustes variances were calculated to estimate disparity, revealing that mid-skeletal stage embryos have significantly reduced skull shape variance relative to all other periods except late-stage embryos.

Table S6. Specimens within CER

List of mid-skeletal period specimens that fall within the CER and which species and ecomorphs they represent. *Gavialis gangeticus* is the single mid-skeletal period embryo which did not overlap this region. Embryos were mostly from existing collections, but *Osteolaemus*, *Alligator*, and *Paleosuchus palpebrosus* were collected for this project and are listed with field ID numbers.

Table S7. Results of global comparison of allometry across species

Results of the Procrustes ANOVA testing whether multiple species specific allometric trends better explain shape data than a single trend for all species using permutation procedures to assess significance. Homogeneity of Slopes test demonstrated that species specific allometric trajectories were significantly different than parallel. These results demonstrate that species do differ in ontogenetic trajectory.

Table S8. Pairwise statistical comparisons of ontogeny

Results of pairwise comparisons of ontogenetic trajectories between species. The outputs of Procrustes ANOVA, Homogeneity of Slopes, and the differences in slope and intercept values of PC1 and 2 projections of the multivariate trajectories between species. Comparisons are broken up to those within the slender ecomorph, within the blunt ecomorph, between the species of Paleosuchus and the blunt ecomorph, and all other comparisons. Parenthetical letters designate the ecomorph of the species (B - blunt, M- moderate, S - slender). P-values were corrected using the Bonferroni correction (bold are significant comparisons). Blunt forms are nearly all indistinguishable in ontogenetic trajectory, but slender forms are nearly all significantly different.

Table S9. PC1 & 2 ontogenetic trajectory coefficients for extant crocodylians

Ontogenetic trajectory variables (slope and elevation) for PCs 1 and 2 for the eighteen (18) species for which embryos or hatchlings were sampled. Values were derived from linear regression of PC scores on centroid size while 95% confidence interval upper and lower bounds were generated using resampling within species.

Table S10. Ancestral state reconstructions for PC1 and PC2 ontogenetic trajectories

Reconstructed values for ontogenetic trajectory coefficients (intercept and slope) for PCs 1 and 2 at ancestral nodes in both the molecular and morphological topologies based on maximum likelihood estimation for continuous variables. Node numbers are those in figure S4 and have been approximately matched with equivalent nodes from the opposing phylogeny. Bold nodes have no real equivalent in the opposing tree.

Table S11. Elevations for ancestral PC1 & 2 ontogenetic trajectories - Molecular

Reconstructed values for PC1 and PC2 ontogenetic trajectory elevations at ancestral nodes in the molecular topology based on maximum likelihood estimation for continuous variables and using

species specific mean sizes to calculate elevation. Extant species differ in mean size, so It is necessary to calculate species specific elevations at each ancestral node to ensure elevation comparisons are based on the same size value. Node numbers are those in figure S4.

Table S12. Elevations for ancestral PC1 & 2 ontogenetic trajectories - Morphology

Reconstructed values for PC1 and PC2 ontogenetic trajectory elevations at ancestral nodes in the morphology topology based on maximum likelihood estimation for continuous variables and using species specific mean sizes to calculate elevation. Extant species differ in mean size, so It is necessary to calculate species specific elevations at each ancestral node to ensure elevation comparisons are based on the same size value. Node numbers are those in figure S4.

Table S13. Heterochronic shifts identified by confidence interval test - Molecular

Reconstructed heterochronic shifts based on comparison of ancestral ontogenetic trajectory coefficients (slope and elevation) to extant species values. Resampling was used to estimate 95% confidence intervals. “NS” means non-significant difference between tip species and ancestral node. Acceleration and deceleration show significant differences in slope while Pre- and Post-displacement show significant differences in elevation. When slopes were significantly different, elevation differences were not considered meaningful. Values used for comparison can be found in Tables S9, S10, and S11. Results are those based on the molecular topology with node numbers matching those in figure S4.

Table S14. Heterochronic shifts identified by confidence interval test - Morphology

Reconstructed heterochronic shifts based on comparison of ancestral ontogenetic trajectory coefficients (slope and elevation) to extant species values. Resampling was used to estimate 95% confidence intervals. “NS” means non-significant difference between tip species and ancestral node. Acceleration and deceleration show significant differences in slope while Pre- and Post-displacement show significant differences in elevation. When slopes were significantly different, elevation differences were not considered meaningful. Values used for comparison can be found in Tables S9, S10, and S11. Results are those based on the morphology topology with node numbers matching those in figure S4.

Supplementary Figures

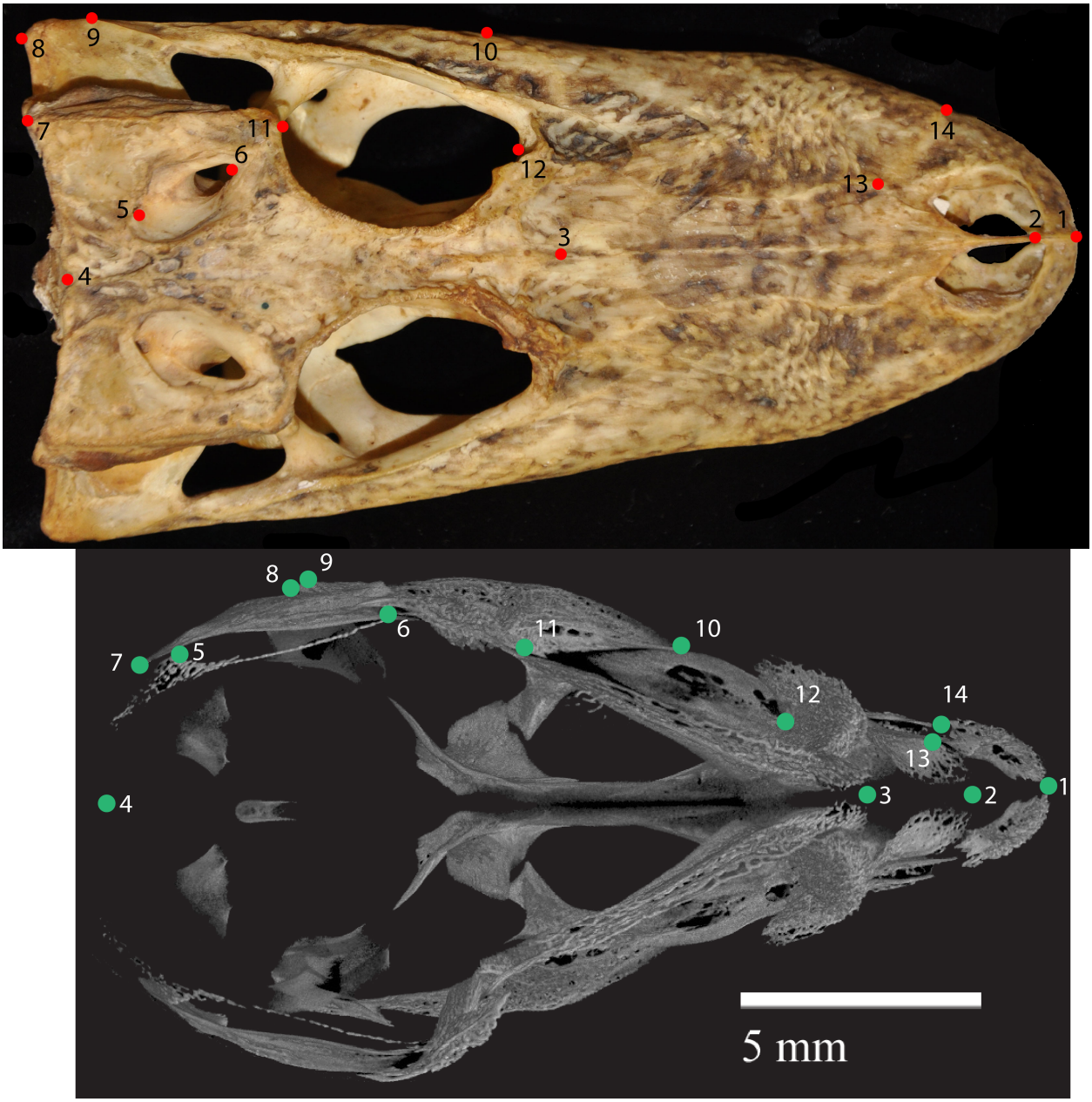

Figure S1. Landmark Positions

Position of landmarks on post-hatching and embryonic specimens. Descriptions of landmarks can be found in Supplementary Methods.

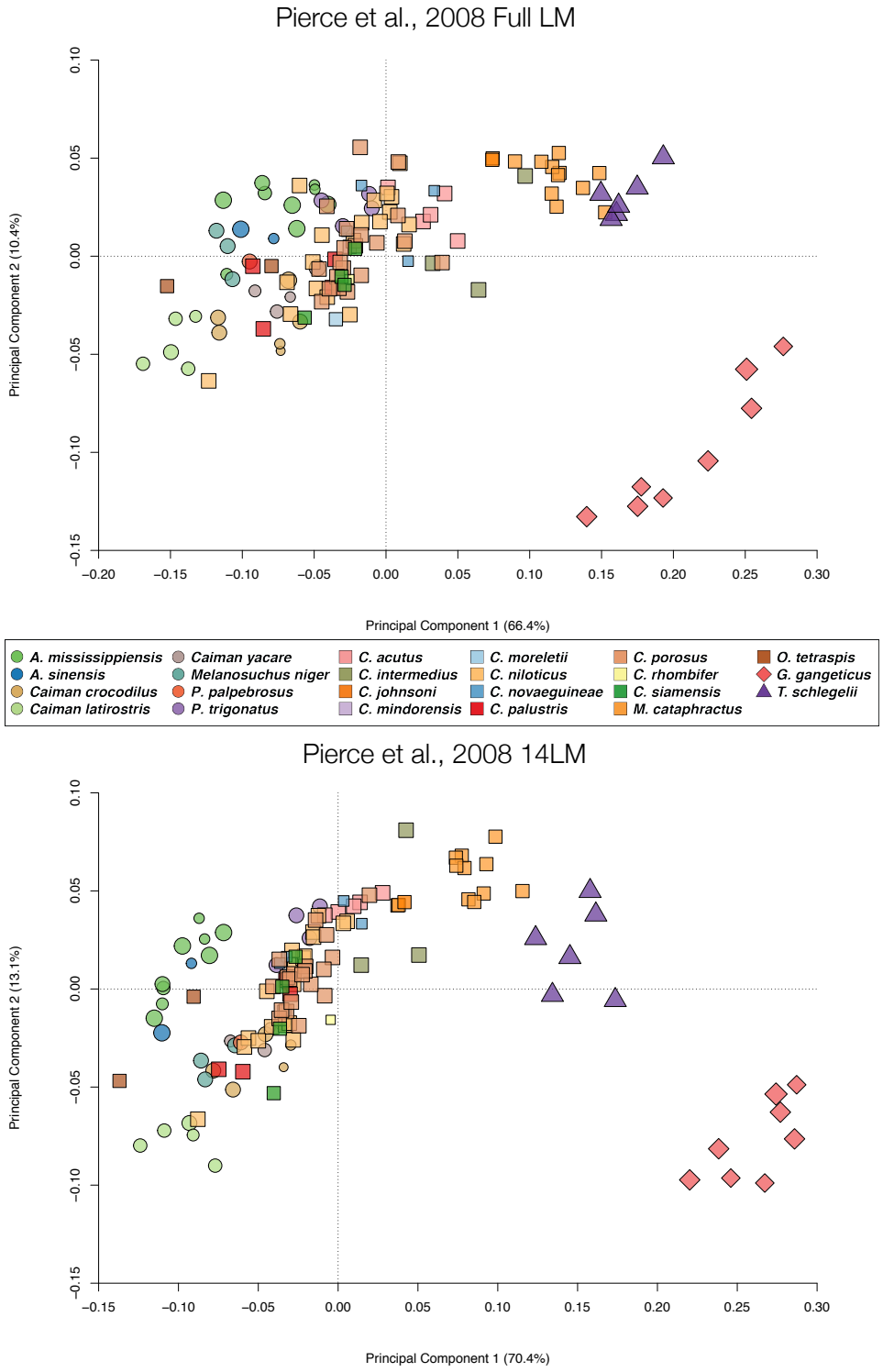

Figure S2. Effect of reducing landmark number on Pierce and colleagues (2008) dataset

Morphospace generated by Pierce and colleagues (2008) using the original full landmark set (top) and after subsampling to match the 14 landmarks included in this analysis (bottom).

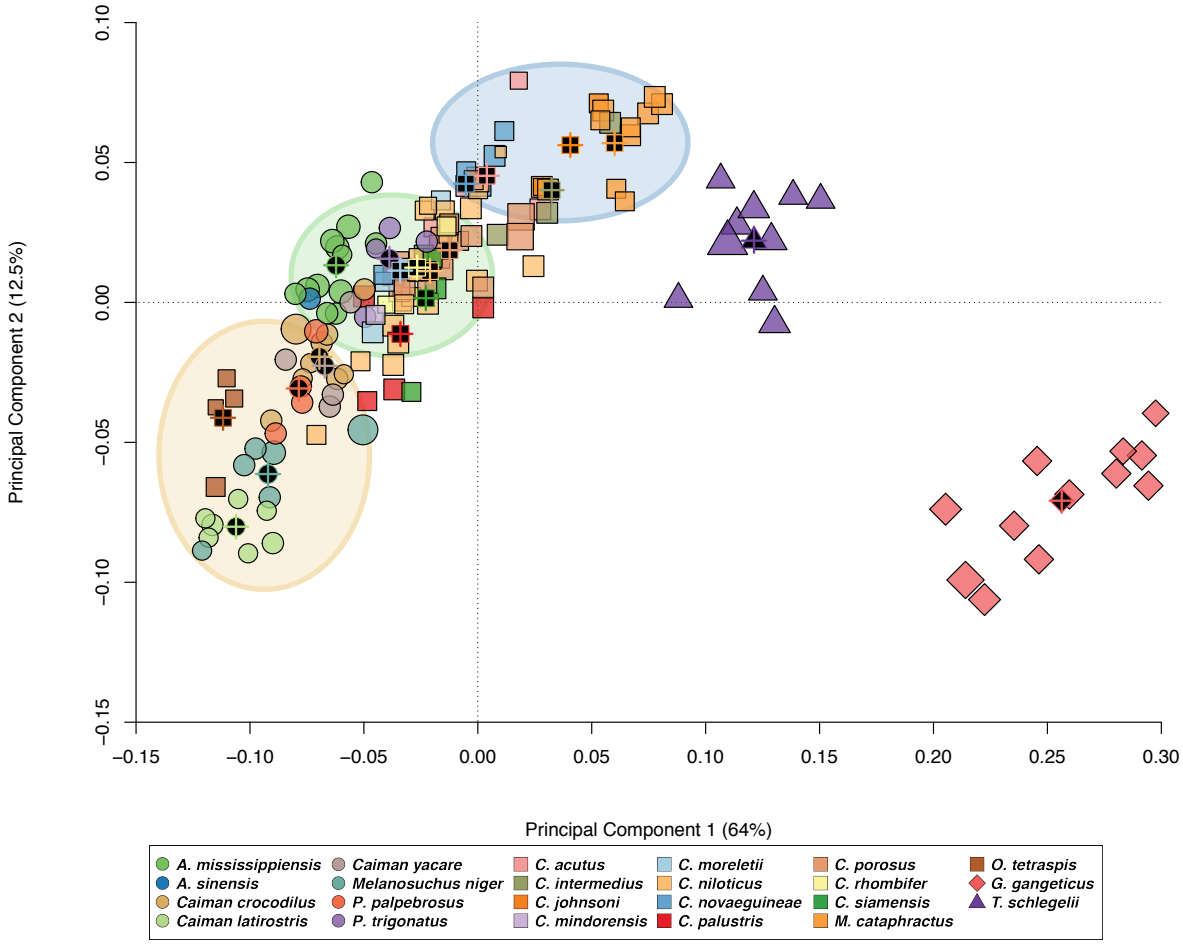

Figure S3. Adults & subadults only morphospace

PCA of adult and subadult specimens for extant crocodylians. We were able to identify groupings corresponding to blunt (tan circle), moderate (green circle), and slender morphotypes (light blue circle). Black symbols with colored crosses display the mean shape for each species. *Tomistoma* and *Gavialis* occupy regions outside those of other taxa but were retained as members of the slender morphotype for the purposes of discussion.

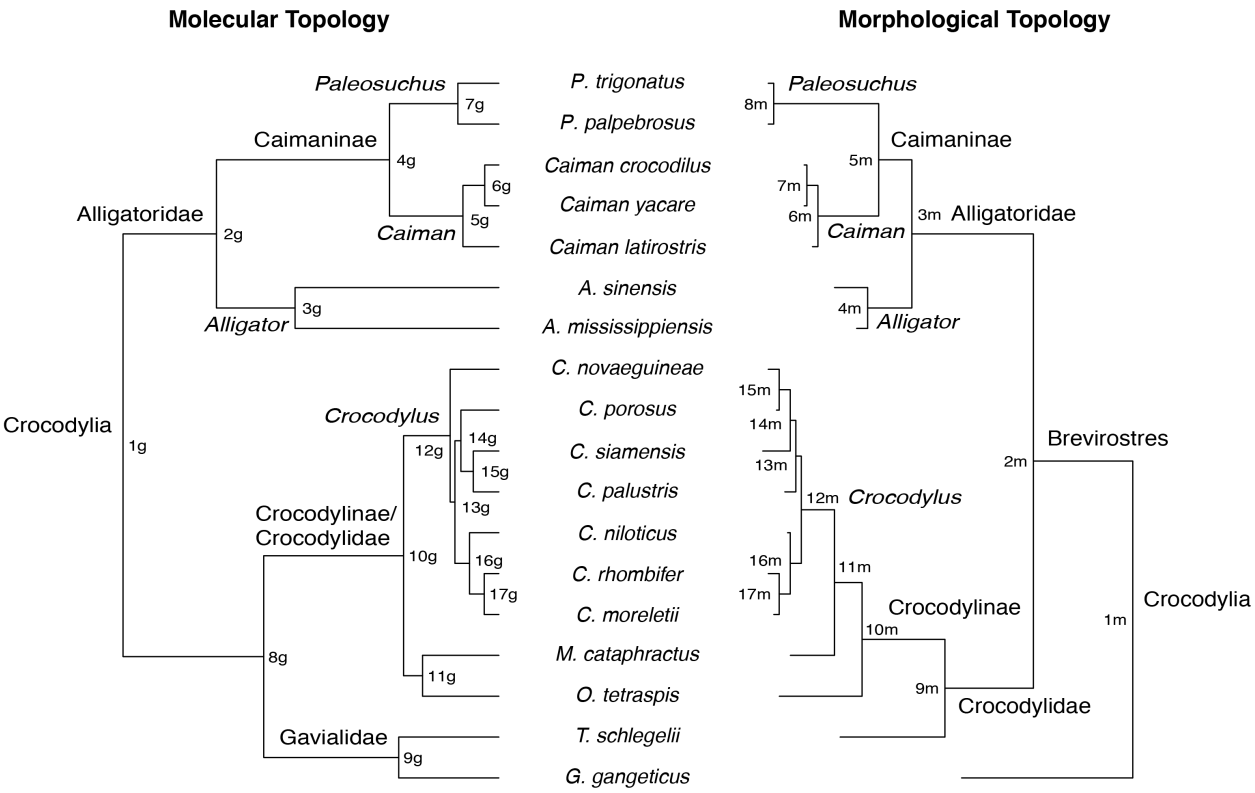

Figure S4. Comparison of morphological and molecular phylogenetic hypotheses

Comparison of the topologies preferred by molecular datasets (Oaks, 2011) and morphological datasets (Narváez et al., 2016) with node numbers and clade names shown. The major differences relate to the position of *Gavialis*, as either the sister taxon to all other crocodylians or sister to *Tomistoma***.** We have chosen to number nodes separately within each tree using “g” to denote the node is in the molecular (a.k.a. the “gene” tree) and “m” to denote the node is in the morphological tropology (a.k.a. the “morphology tree). Some nodes are clearly comparable (e.g., 1g and 1m), where as others only exist in a single tree (e.g., 2m, 8g).

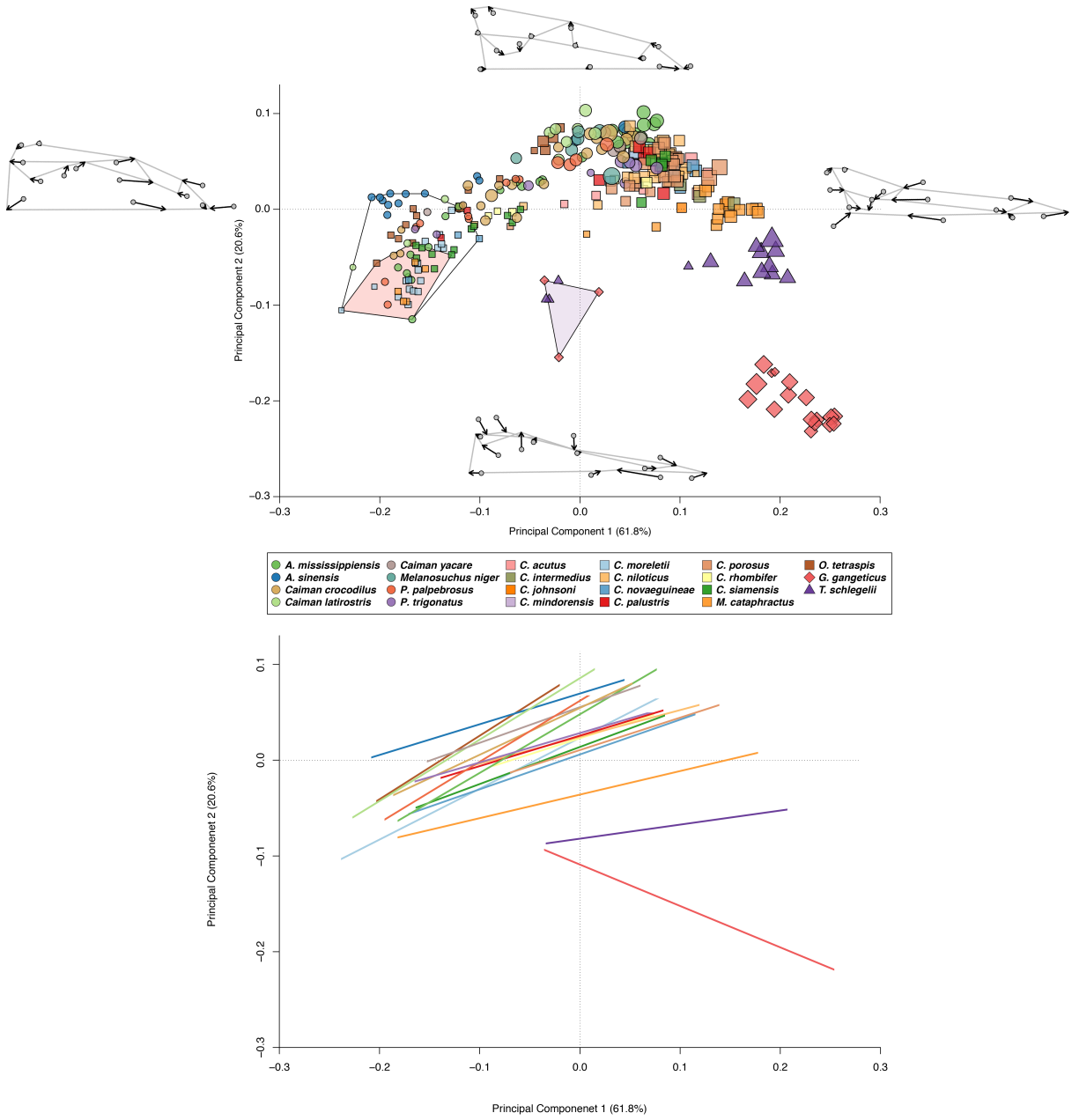

Figure S5. Ontogenetic morphospace with species colors and trajectories

Alternative version of figure 1 in which (top) specimens are colored based on species instead of ecomorph and wireframes show extreme shapes on PCs 1 and 2 and (bottom) species PC1:PC2 trajectories are shown. Wireframes connect the 14 landmarks used in this analysis, displaying the shape of half of the skull in dorsal view with arrows depicting the direction and magnitude of change relative the mean skull shape of the morphospace (i.e., 0,0). Along PC1, positive values correlate with an elongated snout, smaller braincase, and more posterolaterally located orbits and negative values with a short snout, enlarged braincase, and anterior-posteriorly expanded orbits. Along PC2, negative scores correlate with narrow snouts that are straight-sided with retracted nasals and positive values more triangular skulls with wider snouts snouts and more anteriorly extending nasals.

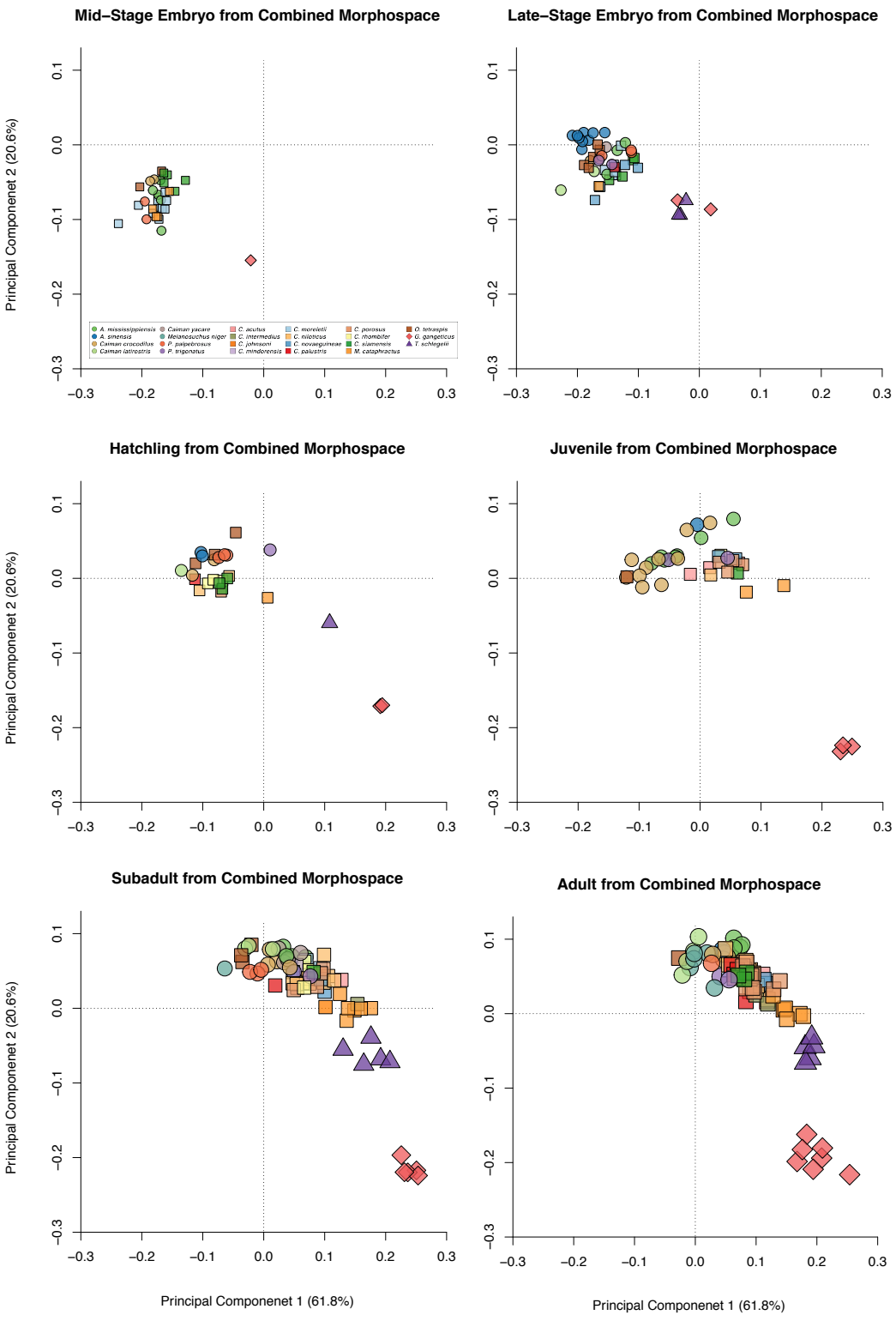

Figure S6. Ontogenetic morphospace subset by developmental periods

Subsets of the total ontogeny morphospace (PC1 vs. PC2) showing only specimens which represent particular developmental periods.

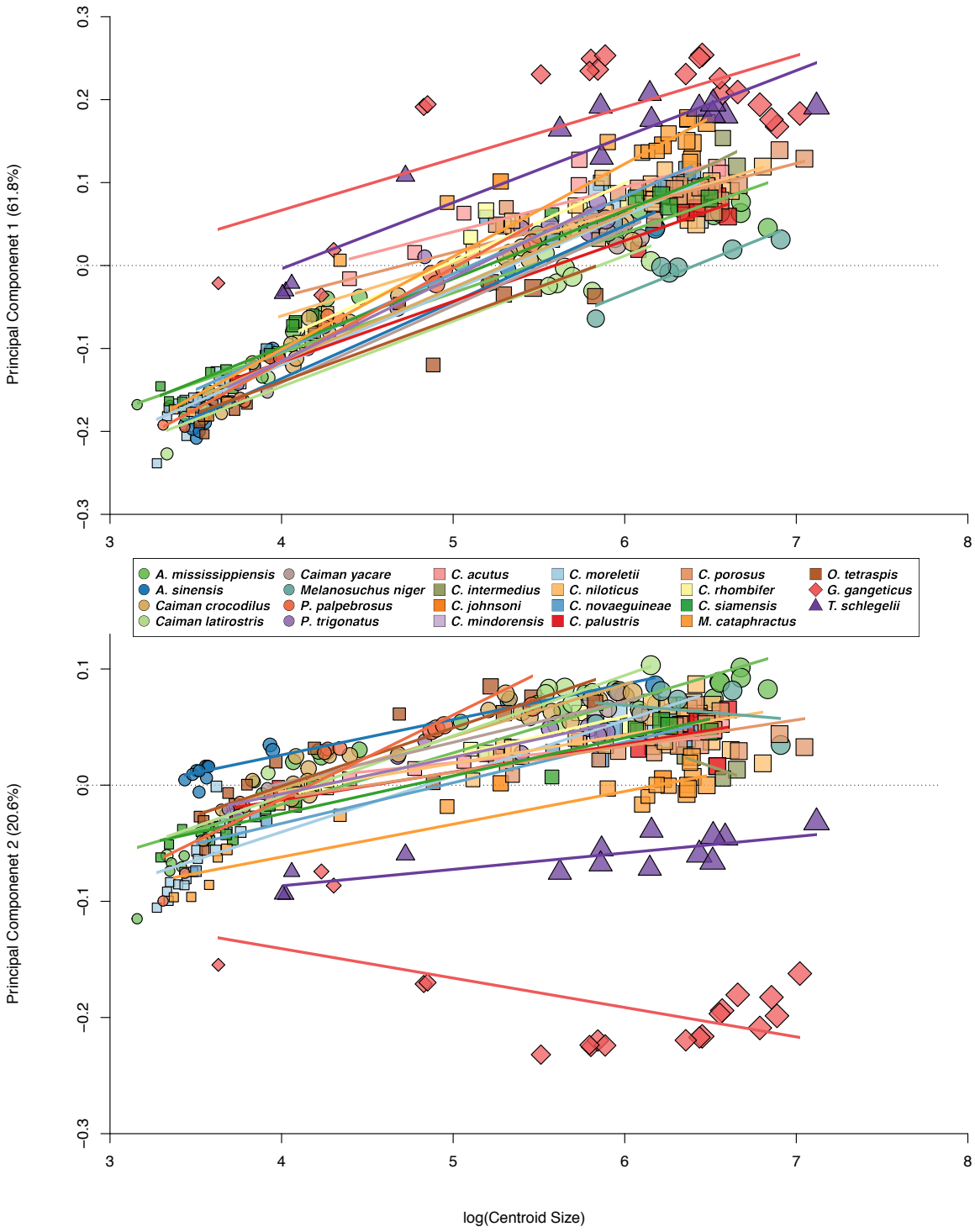

Figure S7. Ontogenetic trajectories for all species

PC1 and 2 projections of ontogenetic trajectories for all species, except those with fewer than 3 specimens (i.e., *Crocodylus johnsoni* and *C. mindorensis*).

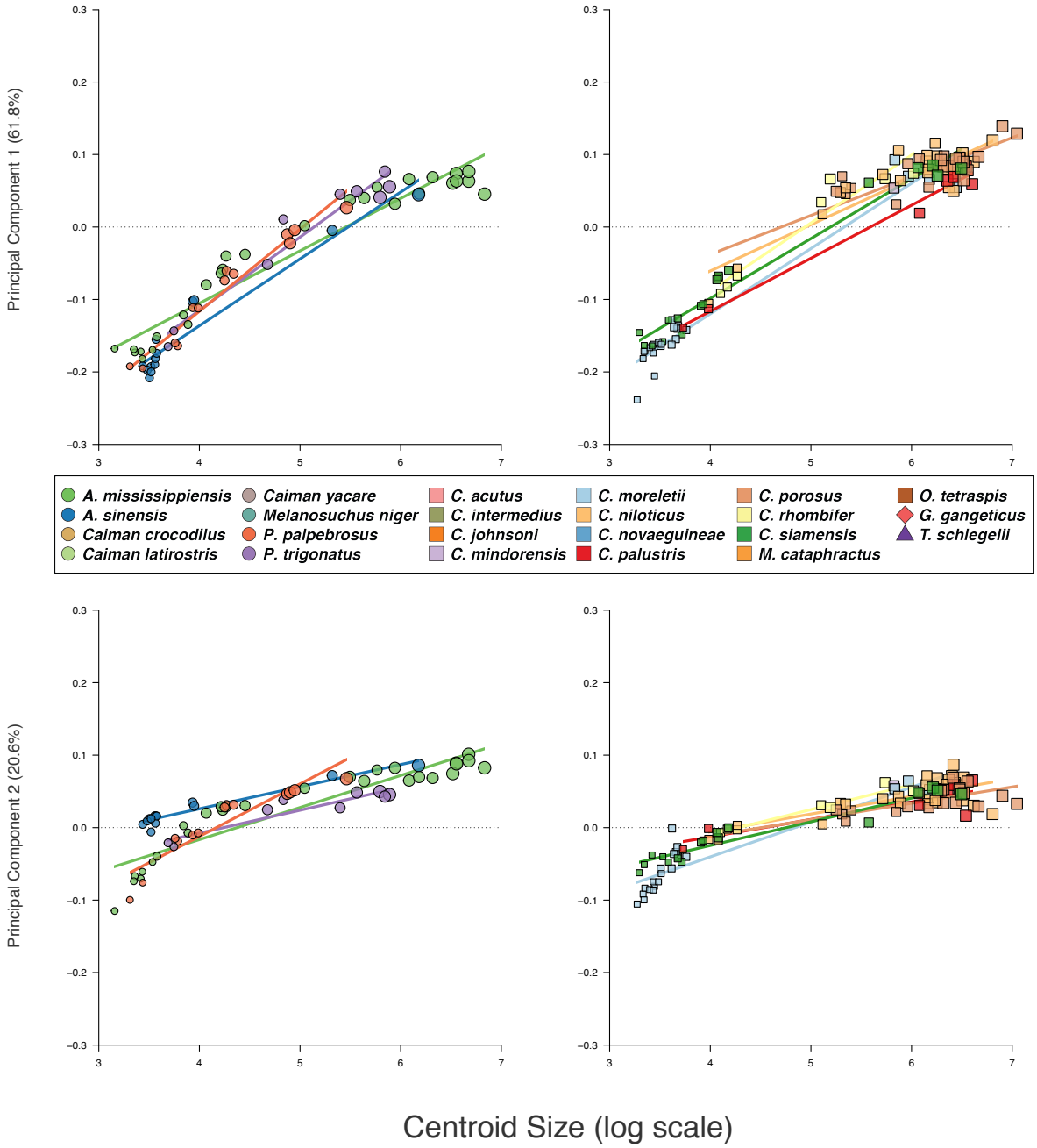

Figure S8. PC 1 & 2 ontogenetic trajectory plots - Moderate

Comparison plots showing PC1 and 2 projections of ontogenetic trajectories for moderate ecomorphs broken into alligatoridae (A,C) and crocodylidae (B,D) clades. All moderate ecomorph species have fairly similar ontogenetic trends, being more variable than blunt and less variable than slender forms.

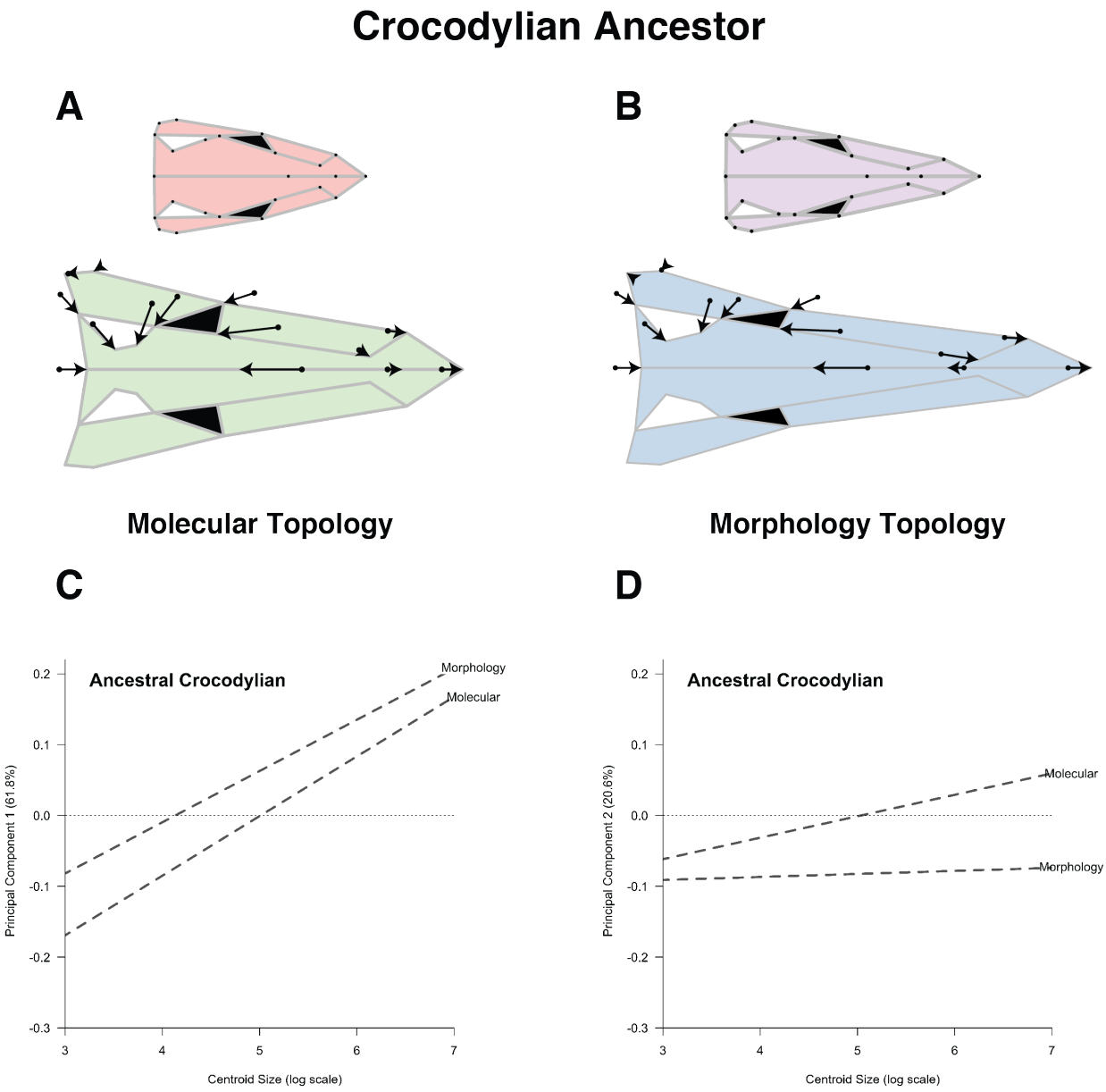

Figure S9. Differences between reconstructions of the ancestral crocodylian ontogeny

Differences between the reconstruction of the ancestral crocodylian ontogeny based on molecular (A) and morphological (B) trees. Reconstructed ontogenetic trajectories projected into PC1 (C) and PC2 (D) show a substantially more slender ontogeny recovered with the morphology topology. The embryonic origins of the molecular topology are well within the CER. The morphology topology suggests a more slender embryonic shape, but still considerably closer to the CER than *Gavialis* and *Tomistoma* embryos.

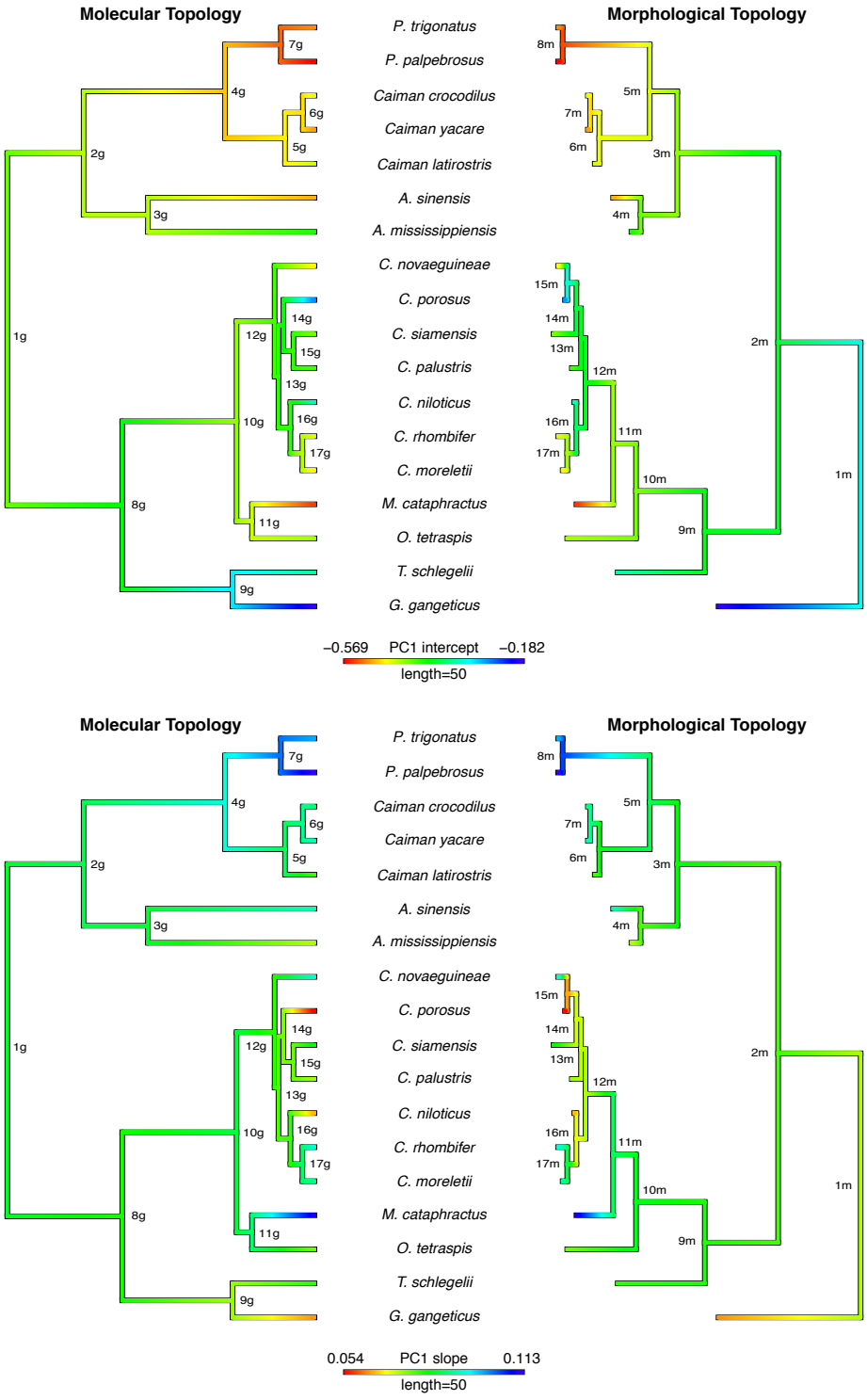

Figure S10. Ancestral state reconstruction of PC1 ontogeny

Phylogenies depicting the ancestral state reconstructions based on maximum likelihood for PC 1 ontogenetic trajectory coefficients (intercept & slope) on molecular and morphological preferred topologies.

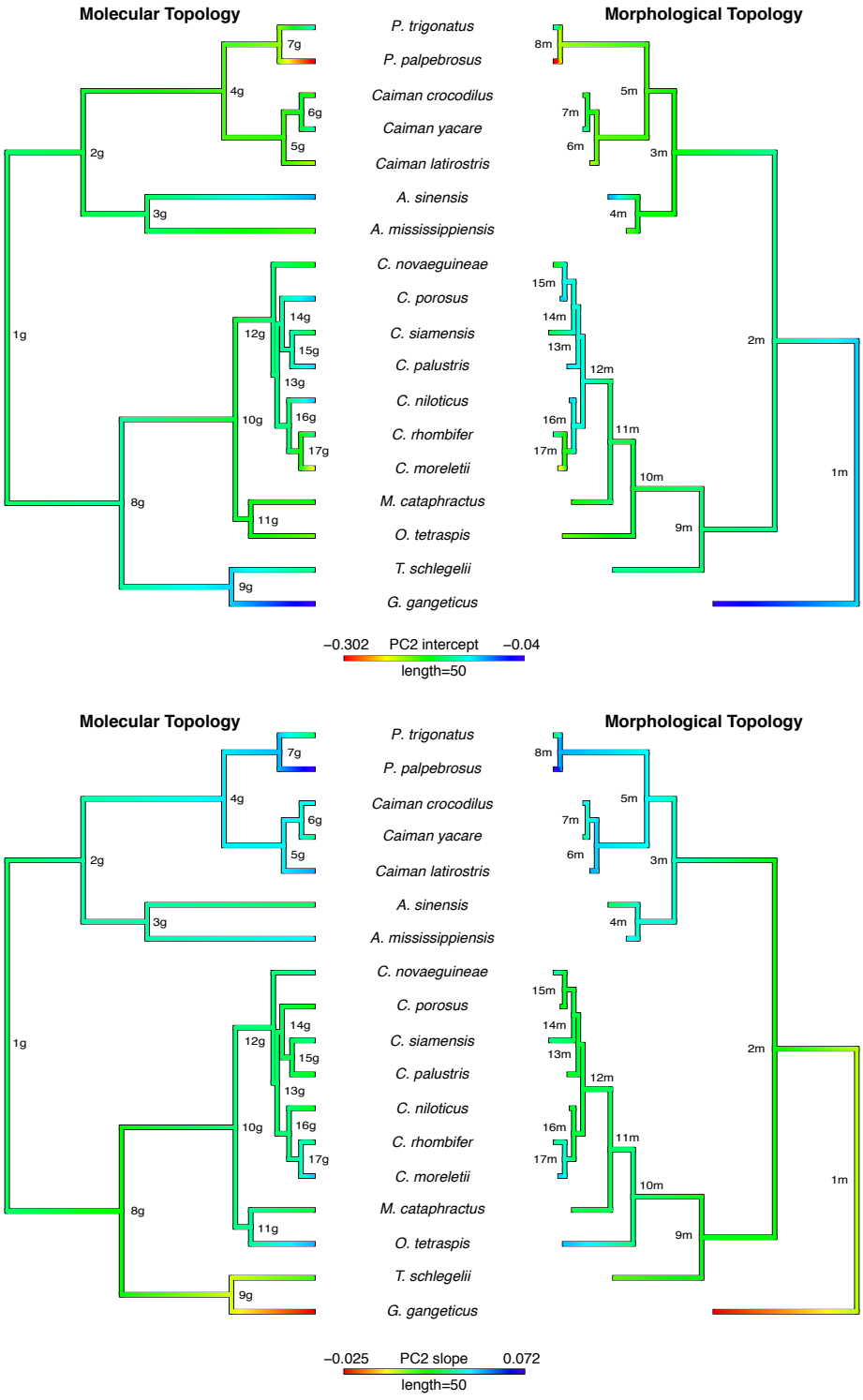

Figure S11. Ancestral state reconstruction of PC2 ontogeny

Phylogenies depicting the ancestral state reconstructions based on maximum likelihood for PC 2 ontogenetic trajectory coefficients (intercept & slope) on molecular and morphological preferred topologies.

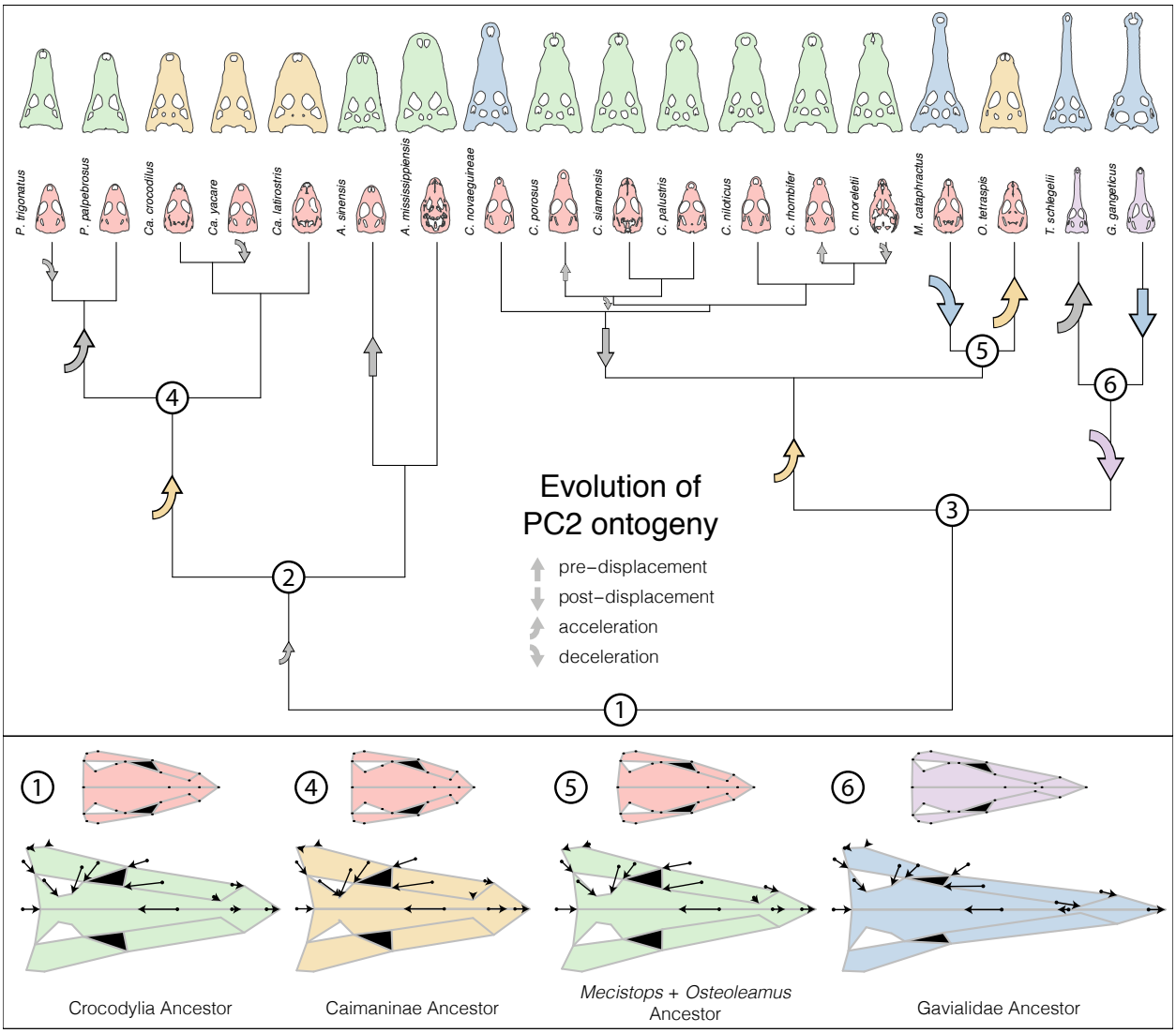

Figure S12. Reconstructed heterochronic modifications to PC2 ontogeny

Reconstructed heterochronic modifications to PC2 ontogenetic trajectories across the crocodylian phylogeny (top panel). Shifts that change adult ecomorph are shown in color of novel ecomorph. Reconstructed embryonic and adult shapes for key ancestral ontogenies are shown (bottom panel) with arrows on the adult shape depicting changes from the embryonic shape. Reconstructed heterochronic modification to PC1 ontogenies can be found in figure 4. A list of heterochrony statements can be found in table S13.

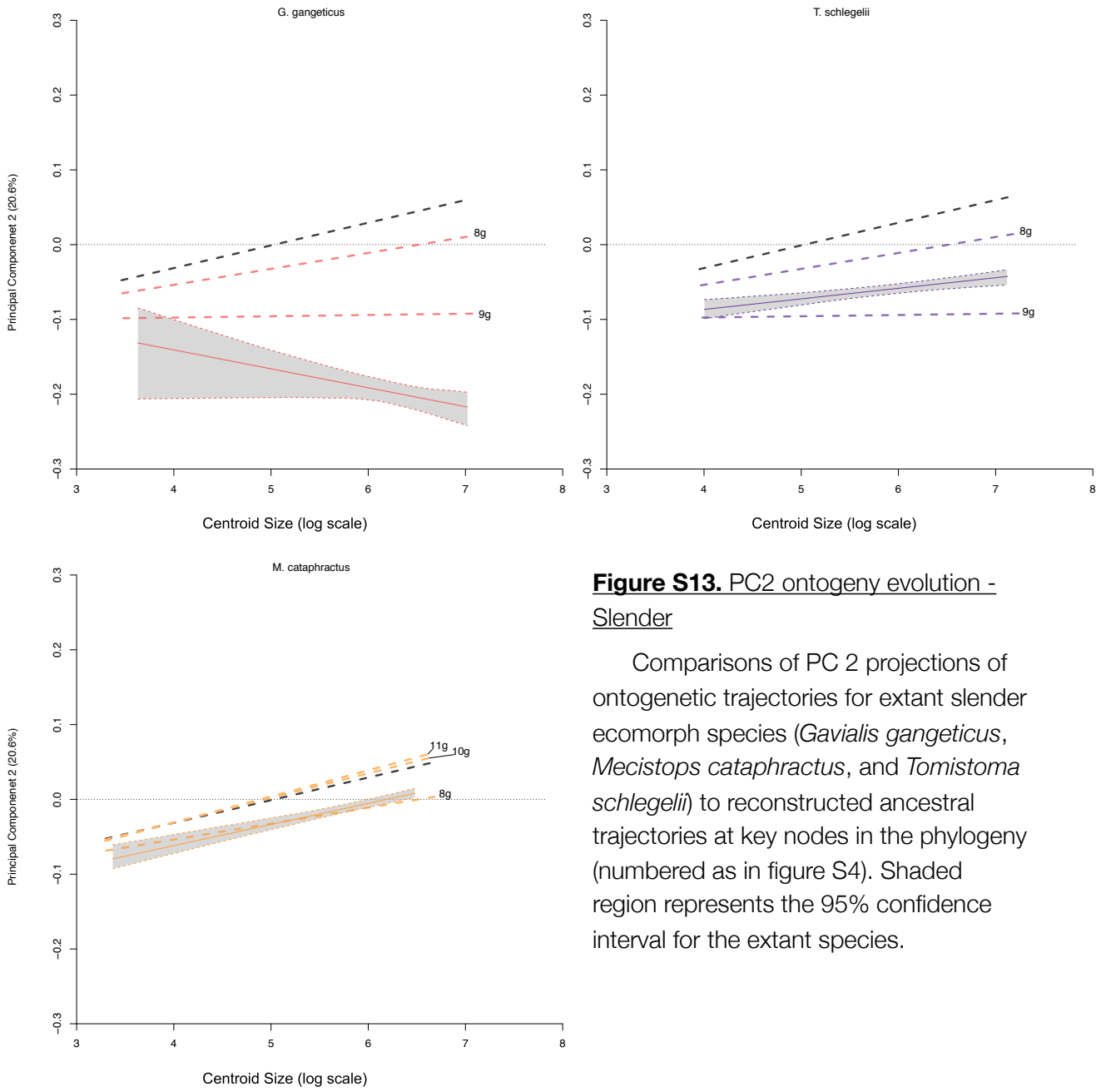

Figure S13. PC2 ontogeny evolution - Slender

Comparisons of PC 2 projections of ontogenetic trajectories for extant slender ecomorph species (*Gavialis gangeticus*, *Mecistops cataphractus*, and *Tomistoma schlegelii*) to reconstructed ancestral trajectories at key nodes in the phylogeny (numbered as in figure S4). Shaded region represents the 95% confidence interval for the extant species.

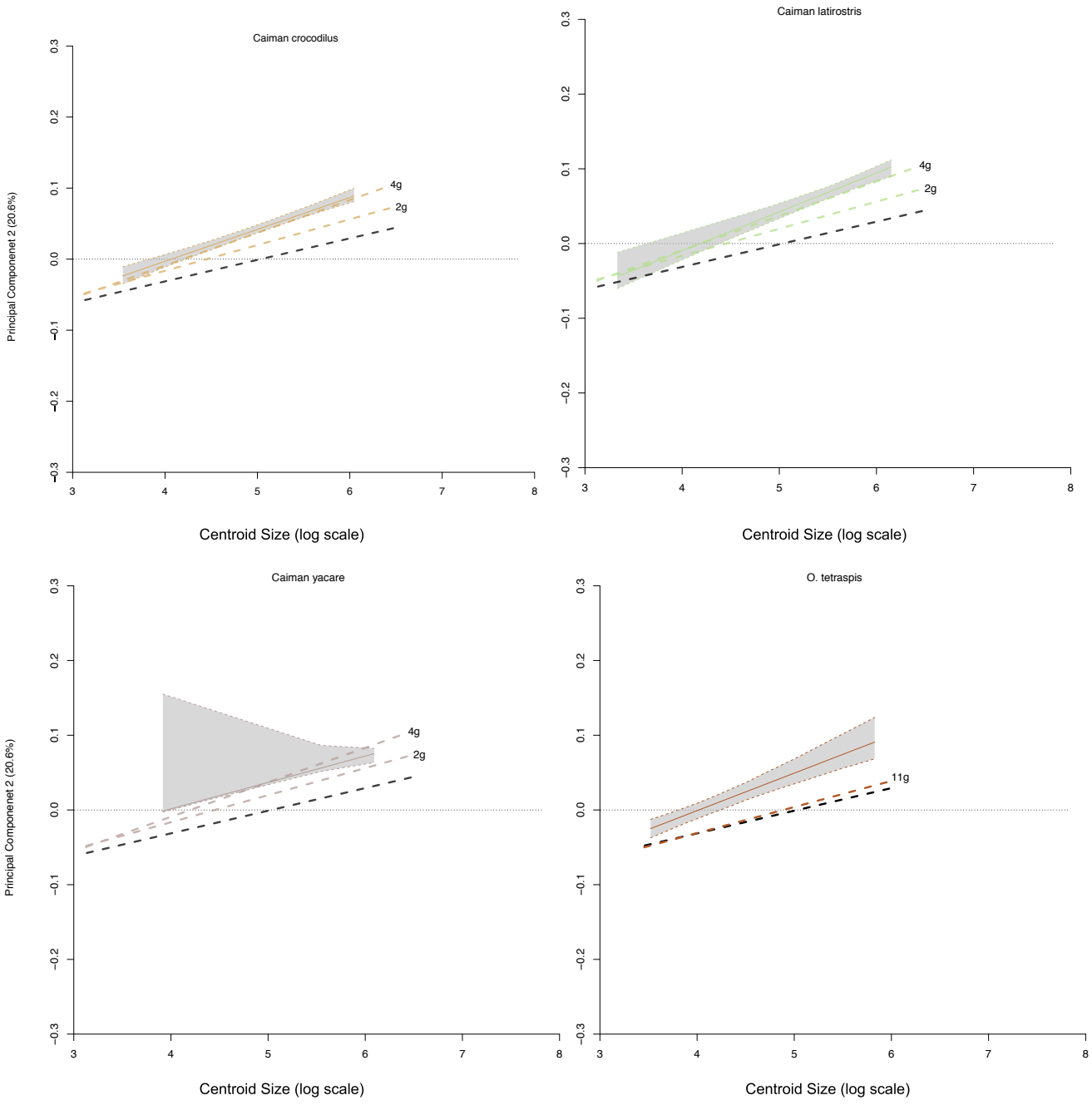

Figure S14. PC2 ontogeny evolution - Blunt

Comparisons of PC 2 projections of ontogenetic trajectories for extant blunt ecomorph species to reconstructed ancestral trajectories at key nodes in the phylogeny (numbered as in figure S4). Shaded region represents the 95% confidence interval for the extant species.